



HAL
open science

Interpretation of the Global Heat of Melting in Eutectic Binary Systems

Yohann Corvis, Philippe Espeau

► **To cite this version:**

Yohann Corvis, Philippe Espeau. Interpretation of the Global Heat of Melting in Eutectic Binary Systems. *Thermochimica Acta*, 2018, 664, pp.91-99. 10.1016/j.tca.2018.04.011 . hal-03022535

HAL Id: hal-03022535

<https://hal.science/hal-03022535>

Submitted on 24 Nov 2020

HAL is a multi-disciplinary open access archive for the deposit and dissemination of scientific research documents, whether they are published or not. The documents may come from teaching and research institutions in France or abroad, or from public or private research centers.

L'archive ouverte pluridisciplinaire **HAL**, est destinée au dépôt et à la diffusion de documents scientifiques de niveau recherche, publiés ou non, émanant des établissements d'enseignement et de recherche français ou étrangers, des laboratoires publics ou privés.

Accepted Manuscript

Title: Interpretation of the Global Heat of Melting in Eutectic Binary Systems

Authors: Yohann Corvis, Philippe Espeau

PII: S0040-6031(18)30112-6
DOI: <https://doi.org/10.1016/j.tca.2018.04.011>
Reference: TCA 77981

To appear in: *Thermochimica Acta*

Received date: 12-6-2017
Revised date: 17-4-2018
Accepted date: 20-4-2018

Please cite this article as: Yohann Corvis, Philippe Espeau, Interpretation of the Global Heat of Melting in Eutectic Binary Systems, *Thermochimica Acta* <https://doi.org/10.1016/j.tca.2018.04.011>

This is a PDF file of an unedited manuscript that has been accepted for publication. As a service to our customers we are providing this early version of the manuscript. The manuscript will undergo copyediting, typesetting, and review of the resulting proof before it is published in its final form. Please note that during the production process errors may be discovered which could affect the content, and all legal disclaimers that apply to the journal pertain.



Interpretation of the Global Heat of Melting in Eutectic Binary Systems

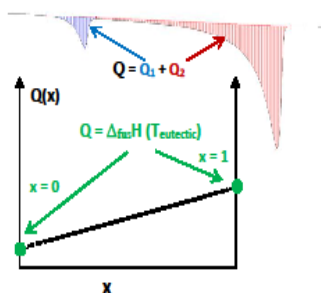
Yohann Corvis, Philippe Espeau*

Unité de Technologies Chimiques et Biologiques pour la Santé, U 1022 Inserm, UMR 8258 CNRS, Faculté des Sciences Pharmaceutiques et Biologiques, Université Paris Descartes, Sorbonne Paris Cité, 4 avenue de l'Observatoire, 75006 Paris, France.

Corresponding Author

* Unité de Technologies Chimiques et Biologiques pour la Santé, U 1022 Inserm, UMR 8258 CNRS, Faculté des Sciences Pharmaceutiques et Biologiques, Université Paris Descartes, Sorbonne Paris Cité, 4 avenue de l'Observatoire, 75006 Paris, France. Phone: +33 1 53 73 96 76. E-mail: philippe.espeau@parisdescartes.fr.

Graphical abstract



Highlights

- Ten eutectic binary phase diagrams are exploited with new thermodynamic approach.
- Heats of melting of binary mixtures are considered from solid state up to melting.
- Linear relationship is found between heat of melting and mole fraction.
- Extrapolated values at $x = 0$ and $x = 1$ are interpreted as melting enthalpies.
- A mathematical model is proposed to explain the experimental data.

Abstract

Starting from ten eutectic binary phase diagrams, the heat absorbed to melt completely a binary mixture from its solid state was plotted as a function of the mole fraction of one of the two components of the system. Surprisingly, a linear relationship was found for all the studied systems. The extrapolated total heat values at pure component composition (*i.e.* $x = 0$ and $x = 1$) obtained via the heat capacity experimentally determined for each compound were interpreted as the melting enthalpies of the pure components at the eutectic temperature, for each binary system. A mathematical model is proposed that takes into account an ideal liquid state and an enthalpy in the liquid state independent of the temperature.

Keywords

Phase diagram, Eutectic system, Thermodynamics, Melting enthalpy, Heat capacity.

1. Introduction

Among all known binary phase diagrams, the eutectic system describes the behavior of two solids that do not mix in the solid state [1, 2]. The two solids in equilibrium at a given temperature may be two solid solutions coming from each pure component of the diagram, where the crystal lattice of a pure component can accept only a limited number of species of the other pure component (and vice versa). In that case we talk about phase diagram with partial miscibility in the solid state. If there is no miscibility in the solid state between both components, the invariant eutectic then goes from $x = 0$ to $x = 1$, and the solids in equilibrium at a given temperature are the pure components [1].

It is well known that, for a eutectic system, the plot of the enthalpy (in $\text{J}\cdot\text{mol}^{-1}$ or $\text{J}\cdot\text{g}^{-1}$) of the eutectic reaction as a function of the composition (mole or mass ratio, respectively) of one component of the mixture is linear on either side of the eutectic point, and the maximum of the enthalpy is obtained at the eutectic point (Tammann plot) [3]. The eutectic reaction occurs at constant temperature, which is why we can talk about enthalpy. Owing to the Tammann plot, the eutectic point as well as the limits of the eutectic invariant can be determined precisely.

In this paper, we were interested in the total heat absorbed by a binary mixture, from its solid state up to melting, that is to say the sum of the heat absorbed during the eutectic

reaction and the heat absorbed when passing through the solid-liquid two-phase domain. It was previously shown that, for a eutectic system involving mixtures of n-alkanes with partial miscibility in the solid state, a linear relationship could exist between the global heat of melting and the composition [4]. For that, a theoretical approach was proposed but never published [4]. Computation of the course of the specific heat capacity as a function of the temperature was also proposed for DSC curves of binary mixtures [5]. A calculation of the “specific enthalpy of fusion of the binary mixtures” led to a linearity of the corresponding plot as a function of the mass fraction of one component. Experimental melting enthalpy *versus* mass fraction has also been reported for the pluronic F127 - ketoconazole system [6]. A linearity of the plot was proposed based only on three experimental points. However, compared to the mean straight line, a deviation of these three points has been noticed.

The aim of this paper is to bring insight into the work initiated in Ref. [4] with the application of the theoretical background to six already published experimental binary systems, involving ten different solid-solid equilibria. Only eutectic systems with complete demixtion in the solid state will be investigated here in order to bring a thermodynamic meaning of the total heat values extrapolated for the pure component compositions ($x = 0$ and 1). Melting enthalpies were calculated at the eutectic temperature, *i.e.* at a temperature different from that of the melting temperature, using the Kirchhoff's law and taking into consideration the specific heat capacity data determined experimentally. The values thus obtained were then compared.

2. Experimental section

2.1. Materials

Table 1 reports suppliers and purities of all the chemical materials used for this work. Moreover, the 1:1 stoichiometric compound between lidocaine and L-menthol (molecular mass: $390.6 \text{ g}\cdot\text{mol}^{-1}$) was prepared as reported in Ref [7]. It is noteworthy that menthol is a polymorphic compound, *i.e.* it can crystalize into different crystalline structures that have *de facto* different physical and chemical properties. In ordinary conditions of temperature and pressure, L-menthol crystallizes in its most stable polymorph called α [8 - 10]. It has been recently demonstrated that pure β L-menthol can be prepared by quenching molten L-menthol from $60 \text{ }^\circ\text{C}$ to lower temperatures (between -80 and $-25 \text{ }^\circ\text{C}$) [9]. For the present study, β L-

menthol was also prepared by thermal quenching of the molten mixtures from 60 to -80 °C. After each heat capacity measurement for β L-menthol, the thus-obtained solid phase was then analyzed by differential scanning calorimetry to certify the 100% purity of the β -menthol prepared samples. The thermograms obtained are presented in supplementary data (Figure S1).

Table 1. Sample purity description

Component	CAS number	Source	Purification method	Final purity (mass %)
Lidocaine	137-58-6	Sigma-Aldrich	None	98.5
L-menthol	2216-51-5	Acros Organics	None	99.7
S-ibuprofen	51146-56-6	Acros Organics	None	99
RS-ibuprofen	15687-27-1	Acros Organics	None	99
Salol	118-55-8	Acros Organics	None	≥ 99
Stearic acid	57-11-4	Alfa Aesar	None	98
Vitamin C	50-81-7	Acros organics	None	99
Acetaminophen	103-90-2	Sigma Aldrich	None	98
D-camphor	464-49-3	Prolabo	sublimation/ condensation [11]	≥ 99
		Acros organics	None	97
DL-camphor	76-22-2	Sigma–Aldrich	None	>98
		Acros organics	None	96
Indium	7440-74-6	Mettler-Toledo	None	99.99
Zinc	7440-66-6	Mettler-Toledo	None	99.99
Water	7732-18-5	–	Millipore [®] filtration	Ultra pure
Naphthalene	91-20-3	Acros organics	None	99

2.2. Thermo-analytical measurements

The differential scanning calorimetry experiments were performed using an 822e and a DSC3 thermal analyzers from Mettler-Toledo (Switzerland). An empty aluminum pan was placed in the reference area. Indium and zinc (purity of 99.99%, Table 1) from Mettler-Toledo, were used for temperature and enthalpy calibration of the DSC devices ($T_{\text{fus}} = 156.6$

$^{\circ}\text{C}$ and $\Delta_{\text{fus}}\text{H} = 28.45 \text{ J}\cdot\text{g}^{-1}$ for indium, and $T_{\text{fus}} = 419.6 \text{ }^{\circ}\text{C}$ and $\Delta_{\text{fus}}\text{H} = 107.5 \text{ J}\cdot\text{g}^{-1}$ for zinc). The DSC samples were weighed in aluminum pans using a microbalance sensitive to $10 \mu\text{g}$ and were hermetically sealed at room temperature.

The thermograms were represented as the evolution of heat flow *versus* the scanned temperature in Celsius degrees. The temperatures were determined at the onset of the signal for the pure compounds. For the binary mixtures, the eutectic temperature was taken at the onset of the first signal, corresponding to the eutectic reaction. The end of the thermal transformation (liquidus or solubility curve) was found out at the extremum of the second signal.

The specific heat capacities (C_{sat}) were measured at saturated vapor pressure by means of the Differential Scanning Calorimeters 822e and DSC3. In order to do so, an experimental procedure was adapted, based on the use of a sapphire reference at a scan rate of $15 \text{ K}\cdot\text{min}^{-1}$ under atmosphere of either dry air or nitrogen (flow rate: $60 \text{ mL}\cdot\text{min}^{-1}$). For each sample, a run was first recorded with an empty aluminum pan topped with its unsealed lid, then a second run was recorded in the same conditions after introducing a translucent sapphire spherical piece (mass $\sim 23 \text{ mg}$ determined with accuracy of $1 \mu\text{g}$) inside the pan, and finally the sapphire was replaced by a known quantity of sample, then the pan was hermetically sealed before recording the third run. The experiments were performed on different samples (up to $n = 6$) and the values were averaged. Temperature ranges were chosen regarding the solid state or the liquid state temperature domain of stability. The mass of each sample was checked after recording the third run. The method was validated with liquid and solid specific heat capacity measurements ($n = 10$) of pure liquid water and ice, respectively. Naphthalene ($n = 6$) was also used to validate the C_{sat} measurements. As far as the heat capacity of liquid water is concerned, the average percentage deviation between our experimental data and two different literature references, namely Osborne *et al.* [12] and Chase [13], was 0.2% for both references (0.4% maximum deviation in both cases). For the heat capacity of ice, the average percentage deviation between our experimental data and two different literature references, namely Osborne [14] and Handa *et al.* [15], was 1.1% and 0.9%, respectively (4.1% and 3.7% maximum deviations, respectively; notably at few low temperatures). For naphthalene, the average percentage deviation between our experimental data and the data reported by Chirico *et al.* [16] was 1.1% and 1.8% for the solid state and the liquid state, respectively (10.5% and 4.8% maximum deviations, respectively; notably at few low temperatures). These comparisons, also proposed as supplementary data (Figures S2 and S3 for water and

naphthalene, respectively), confirm the fact that our experimental C_{sat} determination is quite accurate even if some data will be thereafter compared to other data found in the literature.

The total heat associated to the melting of the solid mixtures was obtained by integrating the DSC curves from the eutectic temperature to the liquidus endset temperature, *i.e.* from the baseline starting before the onset of the invariant peak to the baseline after the endset of the liquidus transformation. All the Q values presented in this work were calculated from published DSC profiles [7, 11, 27-29].

2.3. Theoretical background

Let us consider a eutectic system with partial miscibility in the solid state on both sides of the diagram (Figure 1). At a given composition x , the solid is heated from the solid state (initial state) to the liquid state (final state), assuming that the initial state is located infinitesimally below the eutectic invariant at a temperature $T_{E-\delta}$, and the final state is located at the liquidus point. The initial temperature is constant whatever the composition while the final temperature varies with the composition, since it follows the liquidus curve.

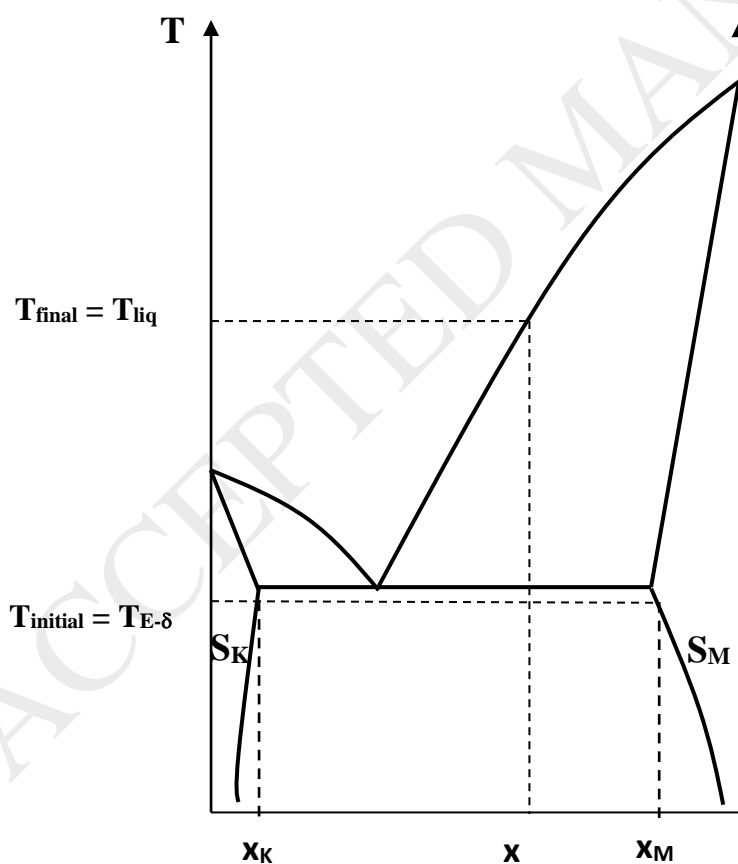


Figure 1. Eutectic system with partial miscibility in the solid state.

The two solid solutions in equilibrium at $T_{E-\delta}$ are S_K and S_M , with respective compositions x_K and x_M . Their associated enthalpies are H_K and H_M (Figure 2).

For a given composition x , the proportion of solid S_K is $(x_M - x)/(x_M - x_K)$ and the proportion of solid S_M is $(x - x_K)/(x_M - x_K)$.

Then, the enthalpy of the system in the solid state $H_{sol}(x)$ is given by:

$$H_{sol}(x) = [(x_M - x)/(x_M - x_K)] H_K + [(x - x_K)/(x_M - x_K)] H_M$$

The final state (liquid state) is assumed to be an ideal state. Then, the associated enthalpy is $H^{liq}(x) = (1-x).H_A^{liq} + x.H_B^{liq}$

This enthalpy will be considered independent of temperature.

However, it has to be noticed that the enthalpy of the liquid sample is not given at the same temperature as the enthalpy of the solid sample. It is the reason why the “enthalpy difference” between both states will be called $Q(x)$.

From $T_{E-\delta}$ to T_{liq} , the sample will absorb a heat quantity equal to: $Q(x) = H^{liq}(x) - H^{sol}(x)$; therefore,

$$Q(x) = (1-x).H_A^{liq} + x.H_B^{liq} - [(x_M - x)/(x_M - x_K)].H_K - [(x - x_K)/(x_M - x_K)].H_M$$

but also

$$Q(x) = H_A^{liq} + (x_K H_M - x_M H_K)/(x_M - x_K) + x.[H_B^{liq} - H_A^{liq} + (H_K - H_M)/(x_M - x_K)] \quad (1)$$

Neglecting the temperature-dependence of H , this relationship is a linear function of x , as represented in Figure 2 (Curve 2). Curve 1 represents the extension of the curve from the solid solutions.

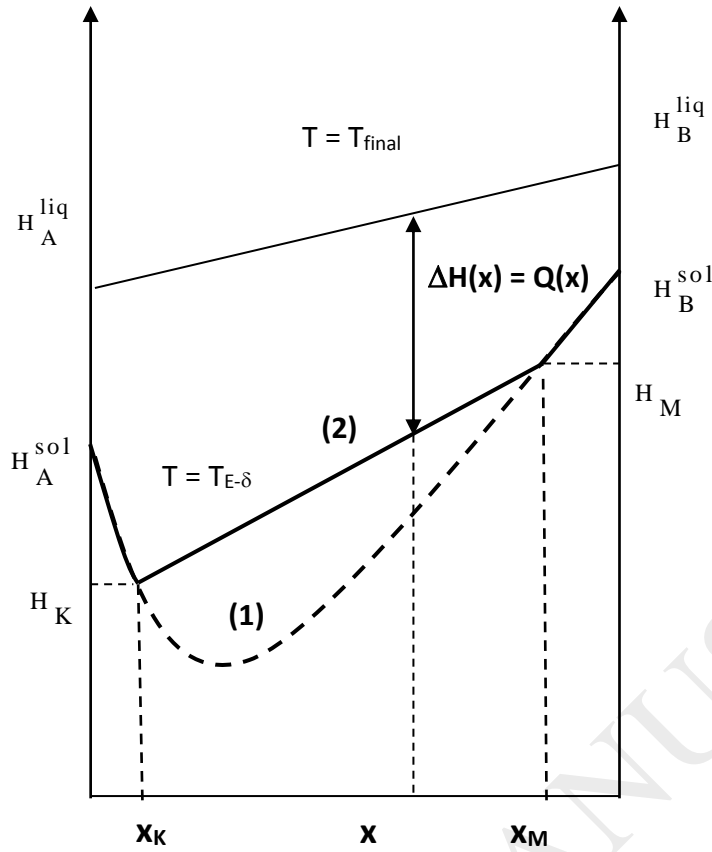


Figure 2. Enthalpy diagram related to the eutectic system presented in Fig. 1

Now, if we consider that the two components are not at all miscible in the solid state, we get a complete demixtion, implying that $x_K = 0$ and $x_M = 1$. It comes out that $H_K = H_A^{sol}$ and $H_M = H_B^{sol}$, that is to say the enthalpies of the pure solids at $T_{E-\delta}$. Consequently, $Q(x) = (1-x) H_A^{liq} + x H_B^{liq} - [(1-x) H_A^{sol} + x H_B^{sol}]$.

Hence, $Q(x=0) = Q_A = H_A^{liq}(T_{fus}(A)) - H_A^{sol}(T_E)$,

and $Q(x=1) = Q_B = H_B^{liq}(T_{fus}(B)) - H_B^{sol}(T_E)$.

These two quantities correspond to the extrapolated values of the straight line whose expression has been established in Eq. (1). As previously said, the enthalpy in the liquid state is not at the same temperature as the enthalpy in the solid state. So, in first approach, Q cannot be directly linked to a melting enthalpy.

To try to give a meaning to these quantities, the Q values will be compared to the melting enthalpies of the corresponding pure component at a given temperature. For that, calculation of $\Delta_{fus}H$ will be done using the following equation (Kirchhoff's law):

$$\Delta_{\text{fus}} H(T) = \Delta_{\text{fus}} H(T_{\text{fus}}) - \int_T^{T_{\text{fus}}} (C_{\text{p,liq}} - C_{\text{p,sol}}) \cdot dT \quad (2)$$

3. Results and discussion

To be able to calculate the melting enthalpy, at different temperatures, of all the pure compounds used in this study, the specific heat capacities were experimentally determined using the experimental procedure based on sapphire reference, as described in the experimental section. The experimental results were fitted using a linear regression, the coefficients of which are reported in Table 2. The relative standard uncertainty of the C_{sat} values was determined in percentage by calculating the average of each C_{sat} ($\Delta T = 1 \text{ }^\circ\text{C}$) standard deviation over the mean C_{sat} (up to $n=6$).

The experimental heat capacity data were tabulated with their corresponding standard uncertainties, as well as the standard relative deviation, as supporting information (from Table S1 to Table S10). Furthermore, the experimental C_{sat} data obtained for the present work regarding seven of the studied compounds were compared to the ones found in the literature. All the comparison graphs are also provided as supporting information for stearic acid, acetaminophen, salol, D-camphor, DL-camphor, S-ibuprofen, and RS-ibuprofen (Figures S4 to S10, respectively).

Table 2. Regression coefficients for the experimental heat capacities (C_{sat}) determined for all the studied compounds: $C_{\text{sat}} (\text{J}\cdot\text{mol}^{-1}\cdot\text{K}^{-1}) = aT + b$, with temperature (T) in Kelvin. The temperature range used is also specified.

		Temperature range ($^\circ\text{C}$)	a ($\text{J}\cdot\text{mol}^{-1}\cdot\text{K}^{-2}$)	b ($\text{J}\cdot\text{mol}^{-1}\cdot\text{K}^{-1}$)	r^2	C_{sat} relative standard uncertainty (%)
L-menthol	Solid α	[-20;32]	1.092 ± 0.008	-68.0 ± 2.1	0.99879	1.3
	Solid β	[-69;-47]	1.041 ± 0.026	-66.4 ± 5.7	0.99333	1.2
	Liquid	[55;77]	1.796 ± 0.021	-195.2 ± 7.2	0.99855	0.6
Lidocaine	Solid	[15;55]	1.280 ± 0.009	-8.3 ± 2.7	0.99911	2.0
	Liquid	[90;130]	0.980 ± 0.012	127.0 ± 4.7	0.99696	1.9
1:1 L-menthol- lidocaine	Solid	[-25;27]	2.463 ± 0.027	-95.5 ± 7.5	0.99689	4.0
	Liquid	[55;93]	2.937 ± 0.056	-131.9 ± 19.4	0.99341	2.9

S-ibuprofen	Solid	[-5;35]	1.589 ± 0.010	-153.3 ± 3.0	0.99837	1.1
	Liquid	[70;105]	1.176 ± 0.012	9.0 ± 4.2	0.99659	1.2
RS-ibuprofen	Solid	[27;63]	1.612 ± 0.006	-181.2 ± 1.8	0.99978	2.7
	Liquid	[100;135]	1.358 ± 0.013	-56.4 ± 5.2	0.99839	1.9
Stearic acid	Solid	[13;48]	3.463 ± 0.041	-528.5 ± 12.4	0.99765	1.1
	Liquid	[85;130]	1.658 ± 0.015	80.7 ± 5.6	0.99826	1.4
Acetaminophen	Solid I	[-25;138]	0.592 ± 0.001	8.7 ± 0.3	0.99979	2.5
	Liquid	[190;237]	0.488 ± 0.007	122.6 ± 3.4	0.99525	1.4
Salol	Solid	[-10;30]	1.039 ± 0.010	-50.7 ± 2.8	0.99822	1.9
	Liquid	[65;105]	0.815 ± 0.012	76.0 ± 4.3	0.99583	1.5
D-camphor	Solid II	[-2;40]	0.561 ± 0.003	80.6 ± 0.8	0.99946	1.0
	Liquid	[193;214]	1.142 ± 0.029	-100.5 ± 7.9	0.99509	0.6
DL-camphor	Solid II	[0;55]	0.441 ± 0.005	112.6 ± 1.4	0.99710	2.8
	Liquid	[189;223]	0.971 ± 0.022	-46.2 ± 4.1	0.99456	3.0

The estimated uncertainties on the regression coefficients are standard uncertainties.

As can be seen in Table 2, the metastable form of menthol (solid β) has lower specific heat values than the stable form (solid α). The difference in heat capacity between both forms is about 6% in the studied range of temperature. This is the consequence of the difference in crystal structure between the two polymorphic forms. It is therefore impossible at this stage to make further comparisons and attempt to find any explanation for these differences since the crystal structure of form β has not been solved until now. However, the same heat capacity hierarchy has previously been reported between the γ form (most stable polymorph) and the α form (metastable polymorph) of glycine [17].

As far as stearic acid is concerned, the C_{sat} values have been previously published for the solid [18] and liquid states [19]. For the solid state, in the 13 – 48 °C temperature range corresponding to our experimental temperature range, one can notice that our values are comparable to those found in Ref. [17] (*cf.* Figure S4 of the supporting information). In the liquid state (Figure S4), a deviation of around 3.5% has been noticed between our experimental values and the data reported in Ref. [19], for C_{sat} values close to the melting point (around 70 °C). Nevertheless, for higher temperatures (50 °C above the melting point), a deviation of 7% was observed between the two sets of values (Figure S4).

For acetaminophen, two references reported C_{sat} determination of the more stable solid phase of acetaminophen [20, 21]. Graphical comparison of the C_{sat} values in the solid state was given in Figure S5 of the supporting information. As a matter of fact, deviations of 3% and 7% were noticed in the solid state between our experimental data and the values given in Ref. [20] and [21], respectively. Figure S6 shows the C_{sat} values for salol, from literature [22] and from this work. Less than 3% of deviation was noticed between our data and the literature values, both in the solid and liquid states. The same difference of 3% between values from the literature [23] and our values was calculated for D- and DL-camphor in the solid state (Figures S7 and S8). It should be noted that if the two experimental sets of heat capacity values for D- and DL-camphor are compared, the same C_{sat} values were found in the solid state, whereas the values in the liquid state differ by ~7%, with higher values for the enantiomeric camphor. This can be explained by the fact that camphor evaporates strongly in the liquid state. That is the reason why the C_{sat} measurements were recorded for the liquid state in a very narrow range of temperature (*i.e.* with a ΔT variation of around twenty degrees). However, we will see that this difference does not significantly affect the enthalpy values calculated from the C_{sat} , and more specifically does not change the conclusions drawn from the extrapolated global heat of melting.

The biggest discrepancies between literature values and our experimental C_{sat} determinations were observed for ibuprofen, both for the enantiomer [24] and the racemic compound [25, 26] (Figures S9 and S10, respectively). Up to 20% difference was observed between the data from Ref. [24] and our set of data in both solid and liquid phases. As far as RS-ibuprofen is concerned, if we take into account the data from Ref. [25], a maximum deviation of 7% was observed in the solid state. It is important to note that the authors of the later reference claim that their reported C_{sat} data concern the *sinister* enantiomer of ibuprofen while they give the CAS number that corresponds to the racemic ibuprofen. Moreover, the melting point reported for their compound corresponds to that of the racemic compound. However, the deviation reached up to 40% for the racemic compound in the solid and the liquid states compared to the data of Xu *et al.* [26].

Although C_{sat} values from the literature concerning ibuprofen may be arguable [24 - 26], the data will nevertheless be used to calculate the extrapolated global heat of melting and the values thus obtained will be compared to the values deduced from our C_{sat} measurements.

The L-menthol/lidocaine system

Stable phase diagram

The α -L-menthol/lidocaine binary system presents a stable eutectic phase diagram with two eutectic points on either side of the equimolar composition, revealing the existence of a 1:1 cocrystal between both components [7]. No miscibility in the solid state was found between this equimolar compound and L-menthol or lidocaine. The experimental eutectic temperatures are $T_{E,1} = 28.6$ °C, and $T_{E,2} = 37.6$ °C for the left- and the right-hand side diagrams, respectively.

In the present work, a linear relationship between the global heats of fusion Q and the mole fraction $x_{\text{lidocaine}}$ was found for each eutectic diagram on both sides of the 1:1 stoichiometric compound composition (Figure 3) by integrating the entire endothermic signal corresponding to the non-isothermal melting of each composition from T_E to T_{liq} . The Q values as a function of the mole fractions and their uncertainties are reported in Tables S11 (left part of the diagram from $x = 0$ to 0.5) and S12 (right part of the diagram from $x = 0.5$ to 1) as supporting information.

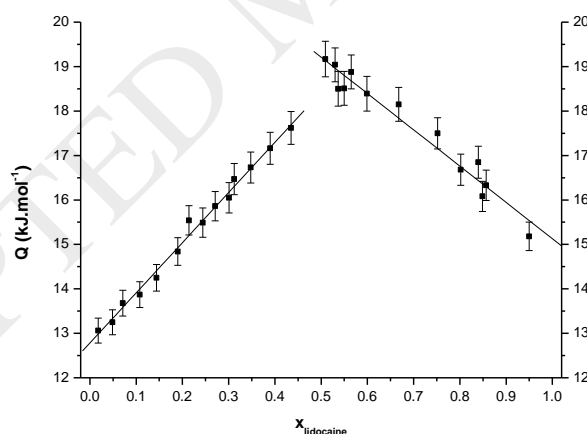


Figure 3. Global heat of fusion for the stable L-menthol/lidocaine binary system as a function of lidocaine mole fraction for each eutectic diagram on both sides of the 1:1 stoichiometric compound composition.

The regression lines intersect for $x = 0.50$ at 36.8 ± 0.1 kJ.mol⁻¹ for the left-hand side diagram, and 38.3 ± 0.4 kJ.mol⁻¹ for the right-hand side one. The global heats of fusion also

obtained at $x = 0$ (pure L-menthol) and $x = 1$ (pure lidocaine) by extrapolation allow us to obtain the respective values of $12.8 \pm 0.3 \text{ kJ.mol}^{-1}$ and $15.1 \pm 0.4 \text{ kJ.mol}^{-1}$.

Using Eq. (2) and the C_{sat} values from Table 2, if we calculate the enthalpy values of the pure compounds and the cocrystal at $T_{E,1}$ and $T_{E,2}$, we obtain the values reported in Table 3. These values are in good agreement with the extrapolated ones determined from the global heats of fusion.

This first result leads us to conclude that, in all cases: i/ linearity of the global heat of fusion vs. mole fraction curve is confirmed and ii/ extrapolated values at the pure component compositions can be assimilated to the melting enthalpy values obtained at the eutectic temperatures, taking into account the C_{sat} influence.

Table 3. Melting data (T_{fus} and $\Delta_{\text{fus}}H$) of lidocaine: α -L-menthol 1:1 stoichiometric compound, α -L-menthol, and lidocaine obtained from Ref. [7], and global heat quantity (Q) obtained by calculus (Calcul.) and also from the extrapolation (Extrapol.) of the two $Q = f(x)$ straight lines at $x = 0, 0.5$ and 1 , for L-menthol, the 1:1 stoichiometric compound and lidocaine, respectively.

	T_{fus} ($^{\circ}\text{C}$)	$\Delta_{\text{fus}}H$ (kJ.mol^{-1})	Q (kJ.mol^{-1})			
			at $T_{E,1} = 28.6 \text{ }^{\circ}\text{C}$		at $T_{E,2} = 37.6 \text{ }^{\circ}\text{C}$	
			Extrapol.	Calcul.	Extrapol.	Calcul.
	from [7]	from [7]				
1:1 compound	39.1 ± 0.1	38.3 ± 0.4	36.8 ± 0.1	37.2 ± 0.7	38.3 ± 0.4	38.1 ± 0.6
α -L-menthol	42.9 ± 0.3	14.1 ± 0.2	12.8 ± 0.3	12.8 ± 0.6	----	----
Lidocaine	68.6 ± 0.5	16.9 ± 0.2	----	----	15.1 ± 0.4	15.7 ± 0.8

The standard uncertainty on the eutectic temperature is estimated at $u(T) = \pm 0.1 \text{ }^{\circ}\text{C}$. The estimated uncertainties on the melting temperatures and enthalpies are standard uncertainties.

The estimated uncertainties on heat quantities (extrapolated and calculated) are standard uncertainties.

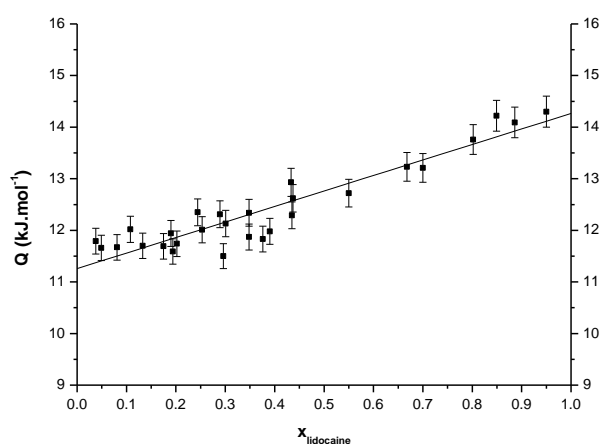
Metastable phase diagrams

Depending on the sample preparation, two L-menthol/lidocaine metastable phase diagrams can also be obtained [7]. The first one involves the α L-menthol polymorph and the other one involves the metastable β L-menthol polymorph with a temperature and an enthalpy of melting equal to 35.7 ± 0.3 °C and 11.2 ± 0.2 kJ.mol⁻¹, respectively [7]. These data were confirmed with two polymorph screening studies conducted first in 2012 [8], then in 2015 [9]. The two later references also give insight into pure β -L-menthol preparation and stabilization.

The eutectic temperature for the system formed between α L-menthol and lidocaine was found to be 12.3 °C. As far as the β L-menthol/lidocaine binary system is concerned, the eutectic temperature is 0.3 °C.

The α L-menthol/lidocaine system

As a matter of fact, the extrapolated value of the global heat at the α L-menthol pure composition is found to be 11.3 ± 0.4 kJ.mol⁻¹ ($T_{E,3} = 12.3$ °C). At the pure lidocaine composition, the corresponding value is 14.3 ± 0.3 kJ.mol⁻¹ (Figure 4A). These results are in agreement with the calculated heat of fusion values at $T_{E,3}$, *i.e.* 11.5 ± 0.7 kJ.mol⁻¹ for α L-menthol and 14.6 ± 0.4 kJ.mol⁻¹ for lidocaine (Table 4).



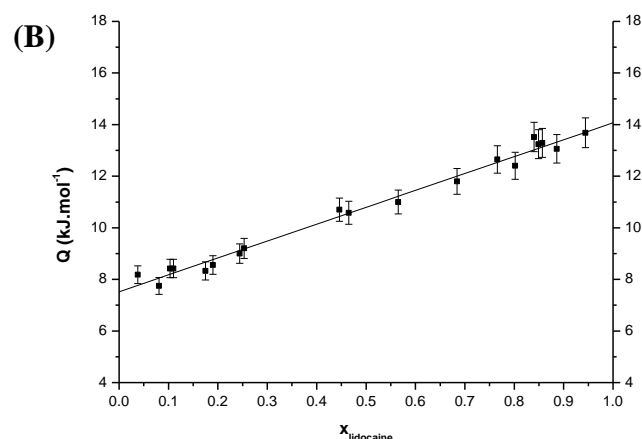


Figure 4. Global heat of fusion as a function of lidocaine mole fraction for the metastable eutectic systems between α L-menthol and lidocaine (A), and β L-menthol and lidocaine (B).

The Q values as a function of the mole fractions and their uncertainties related to Figure 4A and Figure 4B are reported in Tables S13 and S14 respectively (*Cf.* supporting information).

The β L-menthol/lidocaine system

The global heats were obtained at $T_{E,4} = 0.3$ °C for β L-menthol and lidocaine: $Q = 7.5 \pm 0.1$ kJ.mol⁻¹ and 14.1 ± 0.3 kJ.mol⁻¹, respectively (Figure 4B). Besides, the calculated heats of fusion at $T_{E,4}$ were found to be respectively 8.0 ± 0.4 kJ.mol⁻¹ and 14.0 ± 0.9 kJ.mol⁻¹. All the results are gathered in Table 4. As can be noticed, here again, the extrapolated values of Q correlate the calculated heats of fusion at a given temperature.

Table 4. Melting data (T_{fus} and $\Delta_{fus}H$) of α L-menthol, β L-menthol and lidocaine obtained from Ref. [7], and global heat quantity (Q) obtained by calculus (Calcul.) and also from the extrapolation (Extrapol.) of the $Q = f(x)$ straight line at $x = 0$, and $x=1$, for L-menthol, and lidocaine, respectively.

	T_{fus} (°C)	$\Delta_{fus}H$ (kJ.mol ⁻¹)	Q (kJ.mol ⁻¹)			
			at $T_{E,3} = 12.3$ °C		at $T_{E,4} = 0.3$ °C	
	from [7]	from [7]	Extrapol.	Calcul.	Extrapol.	Calcul.
α -L-menthol	42.9 ± 0.3	14.1 ± 0.2	11.3 ± 0.4	11.5 ± 0.7	---	---

β -L-menthol	35.7 ± 0.3	11.2 ± 0.2	---	---	7.5 ± 0.1	8.0 ± 0.4
Lidocaine	68.9 ± 0.5	16.9 ± 0.2	14.3 ± 0.3	14.6 ± 0.4	14.1 ± 0.3	14.0 ± 0.9

The standard uncertainty on the eutectic temperature is estimated at $u(T) = \pm 0.1$ °C. The estimated uncertainties on the melting temperatures and enthalpies are standard uncertainties. The estimated uncertainties on heat quantities (extrapolated and calculated) are standard uncertainties.

The salol/ lidocaine system

The stable phase diagram between salol and lidocaine has been previously determined. It is characterized by a total immiscibility of both components in the solid state, giving rise to a eutectic invariant at $T_E = 18.2$ °C [27]. The melting characteristics of pure salol reported in Ref. [27] are $T_{fus} = 41.9 \pm 0.5$ °C and $\Delta_{fus}H = 19.2 \pm 0.5$ kJ mol⁻¹.

Figure 5 presents the global heat of melting as a function of mole fraction of lidocaine for the salol/lidocaine binary system (corresponding Q values are gathered in Table S15, cf. supporting information). The extrapolated values at $x = 0$ (salol) and $x = 1$ (lidocaine) are respectively 17.6 ± 0.3 and 14.9 ± 0.4 kJ.mol⁻¹, in very good agreement with the calculated values (17.8 ± 0.7 and 14.9 ± 0.9 kJ.mol⁻¹).

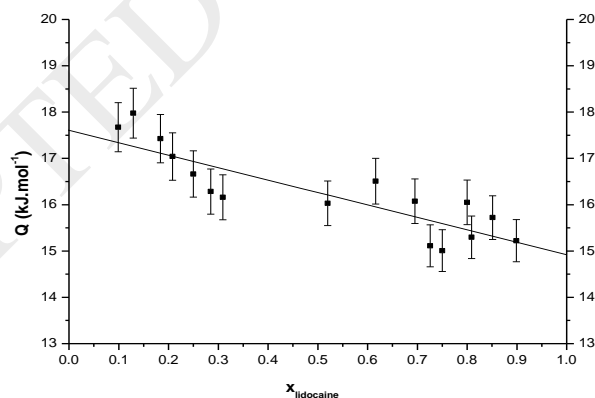


Figure 5. Global heat of fusion as a function of lidocaine mole fraction for salol/lidocaine binary system.

The stearic acid/ibuprofen system

The binary phase diagrams between stearic acid and the *sinister* enantiomer of ibuprofen on the one hand, and the racemic ibuprofen on the other hand, have been previously

established [28]. Melting characteristics of the pure compounds are reported in Table 5. The eutectic temperatures were found at $T_{E,5} = 44$ °C and $T_{E,6} = 57$ °C for the system involving the enantiomer and the other one involving the racemic compound, respectively.

Table 5. Melting data (T_{fus} and $\Delta_{fus}H$) of stearic acid, s- and RS-ibuprofen from Ref. [28], and global heat quantity (Q) obtained by calculus (Calcul.) and also from the extrapolation (Extrapol.) of the $Q = f(x)$ straight line at $x = 0$ for stearic acid and $x = 1$ for ibuprofen.

	T_{fus} (°C)	$\Delta_{fus}H$ (kJ.mol ⁻¹)	Q (kJ.mol ⁻¹)			
			at $T_{E,5} = 44$ °C		at $T_{E,6} = 57$ °C	
			Extrapol.	Calcul.	Extrapol.	Calcul.
Stearic acid	69.2 ± 0.7	61.3 ± 1.3	61.9 ± 0.4	61.0 ± 1.5	59.6 ± 0.4	61.3 ± 1.5
s-ibuprofen	51.6 ± 0.2	18.6 ± 0.3	18.1 ± 1.1	18.4 ± 0.4	---	---
RS-ibuprofen	75.6 ± 0.3	25.5 ± 0.3	---	---	23.8 ± 1.1	24.8 ± 0.4

The standard uncertainty on the eutectic temperature is estimated at $u(T) = \pm 0.1$ °C. The estimated uncertainties on the melting temperatures and enthalpies are standard uncertainties. The estimated uncertainties on heat quantities (extrapolated and calculated) are standard uncertainties.

For both systems, the linearity between the global heat of melting and the mole fraction is also demonstrated as shown in Figure 6. When $x=0$ (pure stearic acid), the straight lines intersect at 61.9 ± 0.4 kJ.mol⁻¹ for the system containing the enantiomer and 59.6 ± 0.4 kJ.mol⁻¹ for the system containing the racemic compound. These values compare well with the melting points calculated values at the eutectic respective temperatures $T_{E,5}$ and $T_{E,6}$: 61.0 ± 2.1 and 61.3 ± 2.2 kJ.mol⁻¹ for the enantiomer and racemic compound systems, respectively (Table 5). As regards the Q values obtained for the pure ibuprofen composition ($x = 1$), 18.1 ± 1.0 kJ.mol⁻¹ was determined for the sinister compound, compared to 23.8 ± 1.1 kJ.mol⁻¹ for the racemic compound. These data are consistent with the global heat calculated using Kirchhoff's law, *i.e.* 18.4 ± 0.4 kJ.mol⁻¹ and 24.8 ± 0.4 kJ.mol⁻¹, respectively.

As for the previous systems, the Q values and their uncertainties are reported in Tables S16 and S17 for the stearic acid/ s-ibuprofen and stearic acid/ RS-ibuprofen systems respectively (Cf. supporting information).

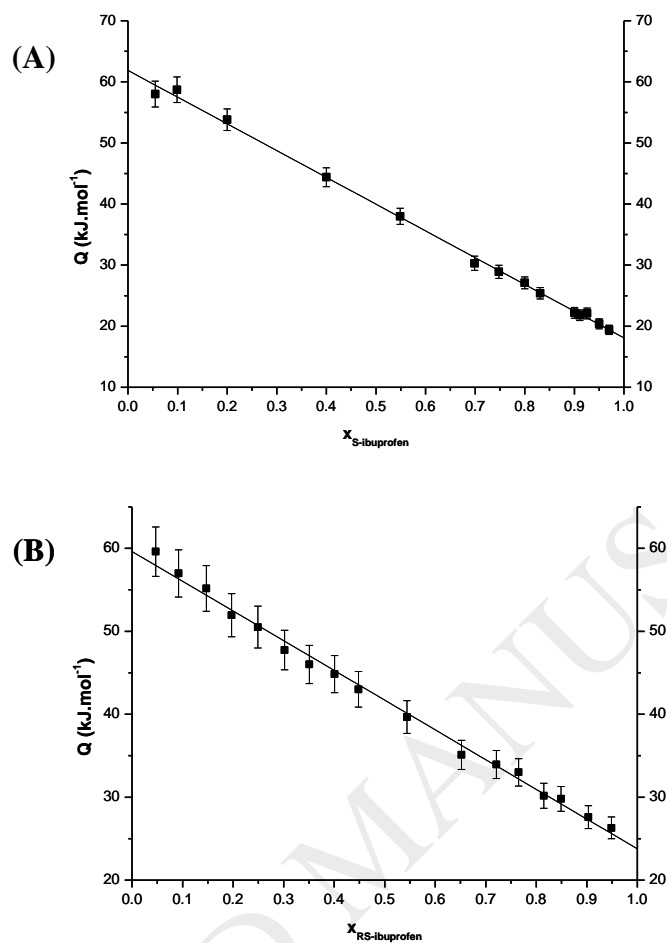


Figure 6. Global heat of fusion as a function of ibuprofen mole fraction for the stearic acid/ibuprofen binary systems. (A) s-ibuprofen, (B) RS-ibuprofen.

As discussed previously in the section devoted to the presentation of heat capacities, ibuprofen C_{sat} discrepancies between our data and those of Xu *et al.* [23, 25] have been highlighted. Although our values seem more consistent with other values from the literature concerning particularly RS-ibuprofen (*i.e.* Di *et al.* [24]), the global heat for s- and RS-ibuprofen has nevertheless been recalculated, taking into consideration the C_{sat} values from Ref. [23] and [25], respectively. Consequently, we obtained $18.3 \text{ kJ}\cdot\text{mol}^{-1}$ instead of $18.4 \text{ kJ}\cdot\text{mol}^{-1}$ for the enantiomer and $24.6 \text{ kJ}\cdot\text{mol}^{-1}$ instead of $24.8 \text{ kJ}\cdot\text{mol}^{-1}$ for the racemic compound. The highest C_{sat} differences noticed for both ibuprofen entities therefore have no impact on the final determination of the global heat.

The vitamin C/acetaminophen system

The particular case of this binary phase diagram is that vitamin C degrades upon melting. The temperature-composition diagram between vitamin C and acetaminophen was established by coupling thermal analysis and analytical experiments in order to fix the liquidus on the vitamin C rich side [29]. Both entities are not miscible in the solid state. This gives rise to a eutectic equilibrium at 152 °C.

The total integration of the DSC curves was performed taking into consideration only the experiments performed at relatively high scan rate, *i.e.* 20 °C.min⁻¹. However, the points on the rich side of vitamin C were not considered since the integration was still accompanied with a too large error due to degradation of vitamin C. The other compositions allowed us to draw the evolution of the global heat of melting as a function of the mole fraction of acetaminophen (Figure 7 and Table S18, *cf.* supporting information).

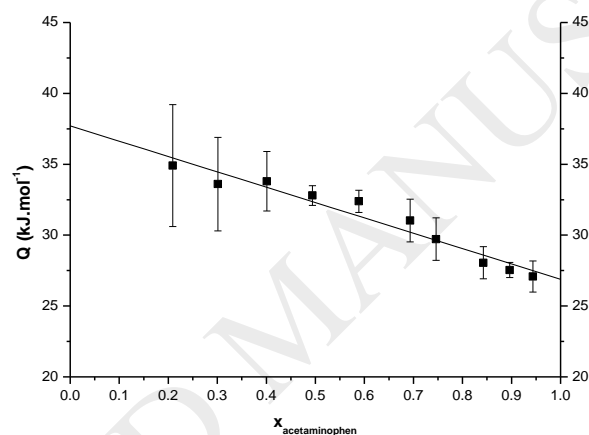


Figure 7. Global heat of fusion as a function of acetaminophen mole fraction for the vitamin C/acetaminophen system.

An extrapolated global heat of melting of 26.9 ± 1.5 kJ.mol⁻¹ was found for acetaminophen at $T_E = 152$ °C, compared to 27.8 ± 1.6 kJ.mol⁻¹ for the acetaminophen heat of melting calculated at the same temperature.

As far as vitamin C is concerned, since this compound degrades upon melting, the heat capacity in the liquid state could not be determined. Consequently, no thermal data at the eutectic temperature could be obtained for this compound. Nevertheless, the global heat of melting extrapolated from Figure 7 at $x = 0$ gives access to $Q = 37.5 \pm 1.5$ kJ.mol⁻¹ at $T_E = 152$ for vitamin C, whereas its melting enthalpy was determined in Ref. [29] as equal to 45.3 ± 0.9 kJ.mol⁻¹ at $T_{fus} = 192.2 \pm 0.5$ °C. Coherently, this value is higher than that obtained at 152 °C.

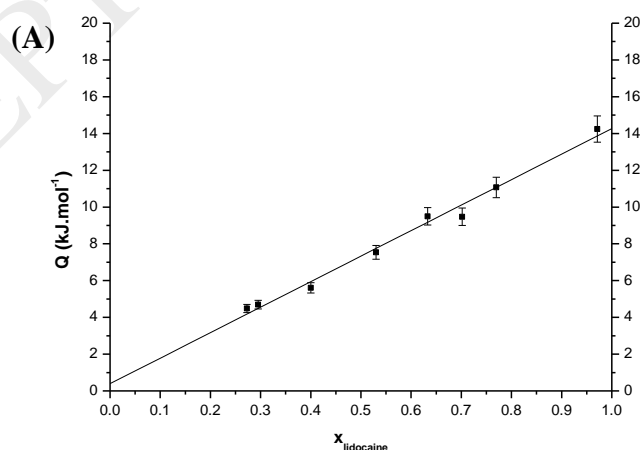
The camphor/lidocaine system

The previously determined phase diagrams between D- or DL-camphor and lidocaine [11] reported a total immiscibility of both components in the solid state with a same eutectic invariant, $T_E = 20\text{ }^\circ\text{C}$, whatever the camphor chirality. Indeed, the D-enantiomer and the racemic compound present almost the same melting characteristics [11]. The two resulting diagrams in the presence of lidocaine are therefore quite the same. Both binary phase diagrams were characterized by a metatectic reaction at the camphor-rich part due to the S_{II} - S_I solid-solid transition exhibited by camphor.

D-camphor melts at $178.8\text{ }^\circ\text{C}$ with an associated melting enthalpy of $6.1 \pm 0.5\text{ kJ}\cdot\text{mol}^{-1}$, and DL-camphor has a melting temperature of $175\text{ }^\circ\text{C}$ and $\Delta_{\text{fus}}H = 6.0 \pm 0.3\text{ kJ}\cdot\text{mol}^{-1}$ [11]. The melting characteristics of the S_{II} solid phase were estimated at $176\text{ }^\circ\text{C}$ with $\Delta_{\text{fus}}H = 6.3 \pm 0.6\text{ kJ}\cdot\text{mol}^{-1}$ for D-camphor and $172\text{ }^\circ\text{C}$ with $\Delta_{\text{fus}}H = 6.2 \pm 0.4\text{ kJ}\cdot\text{mol}^{-1}$ for DL-camphor [11].

Above the metatectic reaction, the liquidus curve corresponds to the solubility curve of S_I solid phase. However, for such a system, the total integration of the heat of melting should take into account the solid phases that co-exist below the eutectic invariant at $T_{E-\delta}$, *i.e.* camphor solid S_{II} and solid lidocaine. As a consequence, one can consider only the points comprised between the richest lidocaine composition of the metatectic invariant and the pure lidocaine composition.

The supporting information files provide Tables S19 and S20, which gather the Q values and their uncertainties as a function of the mole fractions for D-camphor –lidocaine system and DL –camphor –lidocaine system respectively (*Cf.* supporting information).



(B)

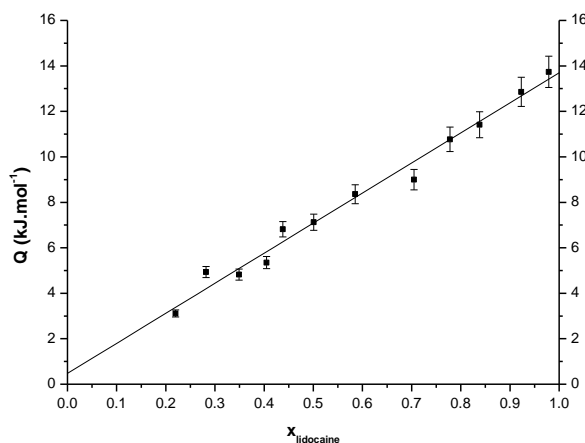


Figure 8. Global heat of fusion as a function of lidocaine mole fraction for camphor/lidocaine systems. (A) D-camphor, (B) DL-camphor.

Regarding the plots of the global heat of melting as a function of mole fraction of lidocaine (Figure 8), the regression lines lead to melting enthalpies of lidocaine, at $T_E = 20\text{ }^\circ\text{C}$, equal to $13.7 \pm 0.9\text{ kJ.mol}^{-1}$ and $14.3 \pm 1.0\text{ kJ.mol}^{-1}$ deduced from the binary systems with D- and DL-camphor, respectively. Besides, from Eq. (2), a value of $14.9 \pm 0.4\text{ kJ.mol}^{-1}$ was calculated at T_E using the C_{sat} values given in Table 1.

For D-camphor (Figure 8A), a value of $0.4 \pm 0.8\text{ kJ.mol}^{-1}$ was extrapolated from the global heat of melting compared to a calculated value of $0.9 \pm 0.7\text{ kJ.mol}^{-1}$. Regarding DL-camphor (Figure 8B), the extrapolated global heat of melting is very similar to the calculated one: $0.5 \pm 0.3\text{ kJ.mol}^{-1}$ and $0.6 \pm 0.5\text{ kJ.mol}^{-1}$, respectively.

Interestingly, the linear extrapolation on the camphor-rich parts of the diagram ($x=0$) leads to a value of $\Delta_{\text{fus}}H = H_{\text{liq}} - H_{\text{cryst}}$ approximately equal to zero, for a temperature of 20°C . This temperature at which a supercooled liquid and a crystalline solid have the same enthalpy, is known as the Kauzmann temperature [30], as schematically drawn in Figure 9. This temperature necessarily locates at a lower temperature than the glass transition point, which can be estimated at $\sim 24\text{ }^\circ\text{C}$ for camphor [30].

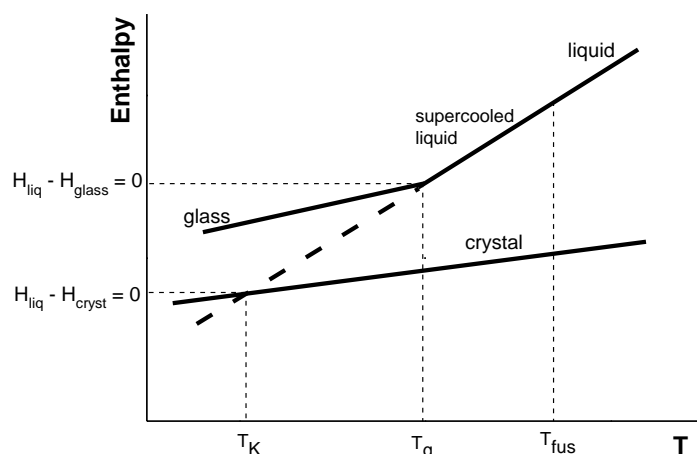


Figure 9. Temperature dependence of the enthalpy of liquid, as well as crystalline and glassy solids.

If we consider all the binary systems of this paper dealing with lidocaine, one can have access to six melting enthalpies of lidocaine at different temperatures. Figure 10 shows the extrapolated and calculated melting enthalpies obtained from the phase diagrams and the specific heat capacity, respectively. In the supporting information, Table S21 reports, as a function of temperature, the melting enthalpy values of lidocaine and their uncertainties, calculated from the specific heat capacities and extrapolated from the binary systems.

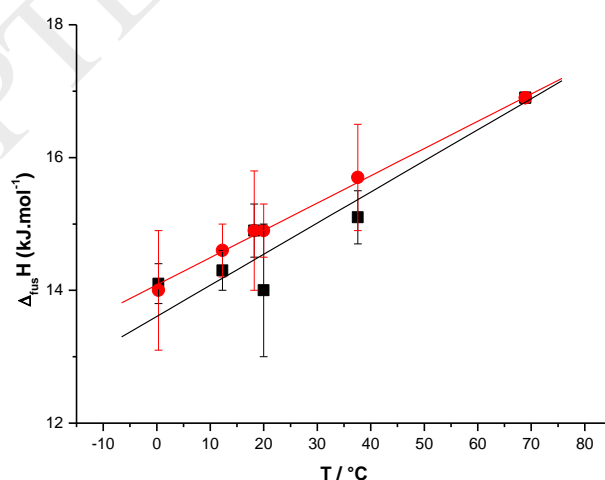


Figure 10. Melting enthalpies of lidocaine as a function of temperature. Red circles: calculated values from the specific heat capacities, black squares: extrapolated values from the binary systems.

This figure validates the interpretation of the extrapolated value as the melting enthalpy of the considered pure compound at the eutectic point. Indeed, for temperatures ranging from 0 to 70 °C, the enthalpy extrapolated from the global heat of fusion and the calculated ones differ by only 2% maximum for lidocaine.

4. Conclusion

Through the ten investigated eutectic systems, it has clearly been shown that the extrapolated values at the pure components composition of the binary system can be associated with the melting enthalpies of the pure components at the eutectic temperature. The proposed mathematical model was formulated taking into account an ideal liquid state and an enthalpy in the liquid state independent of temperature. As a consequence, the enthalpies of the liquid and the solid are not given at the same temperature. Therefore, the mathematical expression established for total heat absorbed does not provide directly a melting enthalpy. But although this model needs to be improved, we have clearly brought the experimental evidence of a linear relationship between the global heat of melting and the mole fraction of one component of the binary system. Since the melting temperature of the pure compounds can be very different from the eutectic temperature, this demonstration has been made possible taking into account heat capacities determined in the solid and liquid states with optimized relative standard deviations. Interestingly, with the binary systems that do not present an ideal liquid state, no significant consequences have been noticed on the linear behavior of total heat absorbed as a function of mole fraction. However, in the case of non-ideal liquid state systems with higher excess Gibbs energy, it would be sufficient to consider only the nearest points of the pure compounds to minimize the influence of excess liquid quantities. It is noteworthy that, for mixtures with high enthalpy of mixing, the linearity will be less pronounced. This would be especially the case with systems in which charge transfer or hydrogen bond formation take place.

Acknowledgement

The authors thank Ms. K. Debbasch for her advice on the manuscript.

References

- [1] H. A. J. Oonk, *Phase Theory: The Thermodynamics of Heterogeneous Equilibria*, Elsevier, Amsterdam, 1981.
- [2] J. C. Zhao, *Methods for Phase Diagram Determination*, Elsevier, Amsterdam, 2007.
- [3] J. Jacques, A. Collet, S. H. Wilen, *Enantiomers, Racemates, and Resolutions*, John Wiley & Sons, New York, 1981.
- [4] P. Espeau, Ph.D. Thesis, University of Bordeaux I, 1995.
- [5] A. Müller, W. Borchard, Correlation between DSC Curves and Isobaric State Diagrams. 1. Calculation of DSC curves from isobaric state diagrams, *J. Phys. Chem. B.* 101 (1997) 4283-4296.
- [6] B. Karolewicz, A. Gorniak, A. Owczarek, E. Zurawska-Plaksej, A. Piwowar, J. Pluta, Thermal, spectroscopic, and dissolution studies of ketoconazole-pluronic F127 system, *J. Therm. Anal. Calorim.* 115 (2014) 2487-2493.
- [7] Y. Corvis, P. Négrier, M. Lazerges, S. Massip, J.-M. Léger, P. Espeau, Lidocaine/L-lenthol binary system: cocrystallization versus solid-state immiscibility, *J. Phys. Chem. B.* 114 (2010) 5420-5426.
- [8] F. E. Wright, Crystallization of menthol, *J. Am. Chem. Soc.* 39 (1917) 1515-1524.
- [9] Y. Corvis, P. Negrier, S. Massip, J.-M. Leger, P. Espeau, Insights into the crystal structure, polymorphism and thermal behavior of menthol optical isomers and racemates, *CrystEngComm* 14 (2012) 7055-7064.
- [10] Y. Corvis, A. Wurm, C. Schick, P. Espeau, New menthol polymorphs identified by flash scanning calorimetry, *CrystEngComm* 17 (2015) 5357-5359.
- [11] Y. Corvis and P. Espeau, Enantiomer versus racemate of camphor: incidence on the phase diagram with an amide type anesthetic compound, *Thermochim. Acta.* 539 (2012) 39-43.
- [12] N. S. Osborne, H. F. Stimson, D. C. Ginnings, Measurements of heat capacity and heat of vaporization of water in the range 0° to 100°, *J. Res. Natl. Bur. Stand.* 23 (1939) 197-260.

- [13] M. W. Jr. Chase, NIST-JANAF Thermochemical tables monograph 9, Fourth ed., J. Phys. Chem. Ref. Data, 1998, 1323-1329.
- [14] N. S. Osborne, Heat of fusion of ice. A revision, J. Res. Natl. Bur. Stand. 23 (1939) 643-646.
- [15] Y. P. Handa, R. E. Hawkins, J. J. Murray, Calibration and testing of a Tian-Calvet heat-flow calorimeter. Enthalpies of fusion and heat capacities for ice and tetrahydrofuran hydrate in the range 85 to 270 K, J. Chem. Thermodyn. 16 (1984) 623-632.
- [16] R. D. Chirico, S. E. Knipmeyer, W. V. Steele, Heat capacities, enthalpy increments, and derived thermodynamic functions for naphthalene between the temperatures 5 K and 440 K, J. Chem. Thermodyn. 34 (2002) 1873-1884.
- [17] V. A. Drebuschak, Yu. A. Kovalevskaya, I. E. Paukov, E. V. Boldyreva, Low-temperature heat capacity of α and γ polymorphs of glycine, J. Therm. Anal. Calorim. 74 (2003) 109–120.
- [18] R. C. F. Schaake, J. C. van Miltenburg, C. G. de Kruif, Thermodynamic properties of the normal alkanolic acids. II. Molar Heat Capacities of Seven even-numbered normal alkanolic acids, J. Chem. Thermodyn. 14 (1982) 771-778.
- [19] F. O. Cedeno, M. M. Prieto, J. Xiberta, Measurements and estimate of heat capacity for some pure fatty acids and their binary and ternary mixtures, J. Chem. Eng. Data 45 (2000) 64-69.
- [20] E. V. Boldyreva, V. A. Drebuschak, I. E. Paukov, Y. A. Kovalevskaya, T. N. Drebuschak, DSC and adiabatic calorimetry study of the polymorphs of paracetamol. An old problem revisited, J. Therm. Anal. Calorim. 77 (2004) 607-623.
- [21] F. Xu, , L. X. Sun, Z. C. Tan, J. G. Liang, T. Zhang, Adiabatic calorimetry and thermal analysis of acetaminophen, J. Therm. Anal. Calorim. 83 (2006) 187-191.
- [22] M. Hanaya, T. Hikima, M. Hatase, M. Oguni, Low-temperature adiabatic calorimetry of salol and benzophenone and microscopic observation of their crystallization: finding of homogeneous-nucleation-based crystallization, J. Chem. Thermodyn. 34 (2002) 1173-1193.
- [23] T. Nagumo, T. Matsuo, H. Suga, Thermodynamic study on camphor crystals, Thermochim. Acta. 139 (1989) 121-132.
- [24] F. Xu, L-X. Sun, Z-C. Tan, R-L. Li, Q-F. Tian, T. Zhang, Low temperature heat capacity of (S)-ibuprofen, Acta Phys. Chim. Sin. 21 (2005) 1-5.

- [25] Y-Y. Di, C-T. Ye, Z-C. Tan, G-D. Zhang, Low-temperature heat capacity and standard molar enthalpy of formation of crystalline (S)-(+)-ibuprofen ($C_{13}H_{18}O_2$)(s), *Indian J. Chem. A* 46 (2007) 947-951.
- [26] F. Xu, L-X. Sun, Z-C. Tan, J-G. Liang, R-L. Li, Thermodynamic study of ibuprofen by adiabatic calorimetry and thermal analysis, *Thermochim. Acta.* 412 (2004) 33-37.
- [27] M. Lazerges, I. B. Rietveld, Y. Corvis, R. Céolin, P. Espeau, Thermodynamic studies of mixtures for topical anaesthesia: lidocaine-salol binary phase diagram, *Thermochim. Acta.* 497 (2010) 124-128.
- [28] Y. Corvis, P. Négrier, and P. Espeau, Physicochemical stability of solid dispersions of enantiomeric or racemic ibuprofen in stearic acid, *J. Pharm. Sci.* 100 (2011) 5235-5243.
- [29] Y. Corvis, M.-C. Menet, P. Espeau, Incidence of the melting-degradation process of vitamin C on the determination of the phase diagram with acetaminophen enhanced by high performance liquid chromatography tools, *New J. Chem.* 39 (2015) 1938-1942.
- [30] W. Kauzmann, The nature of the glassy state and the behavior of liquids at low temperatures, *Chem. Rev.* 43 (1948) 219-256.